Published in final edited form as:
Biomaterials. 2013 November ; 34(33): 8301–8313. doi:10.1016/j.biomaterials.2013.07.013.

Microfabricated polymeric vessel mimetics for 3-D cancer cell culture

Ashley A. Jaeger[a,b,1], **Chandan K. Das**[a,1], **Nicole Y. Morgan**[c], **Randall H. Pursley**[b], **Philip G. McQueen**[b], **Matthew D. Hall**[a], **Thomas J. Pohida**[b], and **Michael M. Gottesman**[a,*]

[a]Laboratory of Cell Biology, National Cancer Institute, National Institutes of Health, Bethesda, MD, USA

[b]Division of Computational Bioscience, Center for Information Technology, National Institutes of Health, Bethesda, MD, USA

[c]National Institute of Biomedical Imaging and Bioengineering, National Institutes of Health, Bethesda, MD, USA

Abstract

Modeling tumor growth *in vitro* is essential for cost-effective testing of hypotheses in preclinical cancer research. 3-D cell culture offers an improvement over monolayer culture for studying cellular processes in cancer biology because of the preservation of cell-cell and cell-ECM interactions. Oxygen transport poses a major barrier to mimicking *in vivo* environments and is not replicated in conventional cell culture systems. We hypothesized that we can better mimic the tumor microenvironment using a bioreactor system for controlling gas exchange in cancer cell cultures with silicone hydrogel synthetic vessels. Soft-lithography techniques were used to fabricate oxygen-permeable silicone hydrogel membranes containing arrays of micropillars. These membranes were inserted into a bioreactor and surrounded by basement membrane extract (BME) within which fluorescent ovarian cancer (OVCAR8) cells were cultured. Cell clusters oxygenated by synthetic vessels showed a ~100um drop-off to anoxia, consistent with *in vivo* studies of tumor nodules fed by the microvasculature. We showed oxygen tension gradients inside the clusters oxygenated by synthetic vessels had a ~100 μm drop-off to anoxia, which is consistent with *in vivo* studies. Oxygen transport in the bioreactor system was characterized by experimental testing with a dissolved oxygen probe and finite element modeling of convective flow. Our study demonstrates differing growth patterns associated with controlling gas distributions to better mimic *in vivo* conditions.

Keywords

Bioreactor; Silicone; Hydrogel; Microstructure; Oxygenation; Carcinogenesis

*To whom correspondence should be forwarded: Michael M. Gottesman, mgottesman@nih.gov, Phone: 301-496-1530, Fax: 301-402-0450.
[1]These authors contributed equally to this work.

Conflict of Interest
The authors declare no conflicts of interest.

1. Introduction

Monolayer cell culture is a widely applied method for studying the biological processes involved in cancer. However, many studies have cast doubt on the ability of monolayer cell culture to adequately recapitulate complex features of the tumor microenvironment, with well-documented differences in cell morphology, metabolism, migration, signaling, gene expression and differentiation [1–8]. These differences have been attributed to discrepancies between two-dimensional (2-D) culture and the three-dimensional (3-D) tumor environment, including substrate architecture and rigidity [1, 9], the effect of neighboring, non-malignant cells *in vivo*, including vasculature and immune cells [10], the nature of cell clones that adapt to culture conditions [5], and environmental conditions of conventional cell culture [6] such as nutrients, growth hormones, and O_2 tension — none of which replicate the pathophysiology of tumors [9, 11, 12]. The development of *in vitro* culture systems that more closely mimic the tumor microenvironment along one or more of these directions, potentially yielding more biologically relevant data, is therefore highly desirable.

3-D cell culture is thought to offer an improvement over monolayer culture, as it preserves cell-cell and cell-extracellular matrix (ECM) interactions that affect cellular phenotype, gene expression, and a range of cellular functions [9, 13–17]. Cell–ECM interactions are fundamental to tumorigenesis, suggesting that 3-D culture offers improved physiological modeling of tumor angiogenesis, metastasis, and invasion over traditional cell culture. Although animal models can provide a representative microenvironment, they are not scalable for high-throughput screening and may not accurately reproduce features of human tumors and drug responses [9]. Bridging the gap between monolayer cultures and animal models, 3-D tissue engineering will be an essential tool in future cancer research and drug development studies [2, 12, 18]. Common 3-D cell culture models for cancer research include the use of organotypic explants [19, 20], and cells grown in 3-D scaffolds [11], PEG hydrogels [21, 22] or collagen gels [23, 24]. Multicellular tumor spheroids (MCTSs), the most widely used approach, are grown in suspension [25–27] or embedded in cell-secreted [28] or naturally derived [29–32] extracellular matrix (ECM).

The lack of vasculature in 3-D cell culture poses a significant barrier to engineering extended tissue constructs and mimicking *in vivo* molecular gradients [25, 27, 33]. As cultured tumor cells grow into larger organotypic structures, the transport of O_2, nutrients, and cell by-products is insufficient for sustaining metabolism and growth, causing a gradient of hypoxia, acidosis and eventual necrosis. Most spheroid tumor models exhibit molecular gradients similar to the microenvironments of micrometastases and avascular tumor nodules, developing central hypoxia and necrosis as the spheroid enlarges beyond a critical size of approximately 400–600 μm [34, 35]. This architecture is distinct from vascularized tumors, where tumor cells surround vessels in the microvasculature, and peripheral cells are hypoxic due to diffusion limitations [26, 34, 35]. Given the central role of the microvasculature in supplying and limiting growth, we hypothesized that mimicking vessels by using micropillars to facilitate delivery of O_2 to surrounding cells would be more reflective of the *in vivo* tumor microenvironment.

Slowly proliferating tumor cells, such as those seen at greater distances from a blood vessel, are more likely to exhibit drug resistance, particularly towards cell-cycle specific toxins. However, tumor cells grown in artificial cellular environments at conventional O_2 tensions are highly proliferative, affecting cell behavior. These differences likely contribute to the discrepancies observed between *in vitro*- and *in vivo*-based drug testing. In order to obtain more clinically-relevant data and better predict efficacy of chemotherapeutics, it would be advantageous to mimic oxygenation conditions when developing drug assays and tumor models.

In this report, we describe a system developed to facilitate gas exchange and mimic *in vivo* oxygenation gradients in cancer cell organotypic cultures. Our approach, shown schematically in Fig. 1A, utilizes a silicone hydrogel material with high O_2 transmission properties [36]. Silicone hydrogel polymers offer wettability and allow O_2 transport comparable to purely hydrophobic counterparts such as polydimethylsiloxane (PDMS) [37, 38]. Silicone hydrogel was cast into a membrane with high aspect ratio micropillar structures, and incorporated into a bioreactor culture system (Fig. 1B) designed to deliver O_2 through the hydrogel pillars into an otherwise hypoxic environment. Based on finite element modeling of oxygen transport in the system, these micropillars are expected to act as oxygen sources for surrounding cells, giving rise to oxygenation gradients on the length scale of the microvasculature. A human ovarian cancer cell line stably transfected with the red fluorescent protein DsRed2 (OVCAR8-DsRed2) was cultured in Matrigel surrounding these pillars. We demonstrate differing cell growth patterns associated with mimicking *in vivo* O_2 distribution.

2. Materials and methods

2.1 Design and construction of bioreactor system

The bioreactor system was designed in 3-D computer aided design (CAD) modeling software (SolidWorks, Waltham, MA). The subsequent fabrication of the various components was accomplished with either a Dimension Elite 3-D printer (Stratasys, Eden Prairie, MN) or a VLS3.50 50 W CO_2 laser cutting tool (Universal Laser Systems, Scottsdale, AZ). In the case of the laser cut components, we used ¼”-thick cell cast acrylic sheets (Arkema, King of Prussia, PA), and the parts were assembled primarily with acrylic solvent (Weld-On #4, IPS Corporation, Compton, CA). Basic bioreactor system design requirements included: (1) a non-pressurized bottom gas chamber allowing flow-through mixed gases, (2) a non-pressurized top chamber to hold cell growth media and anoxic gas flow-through to serve as an O_2 sink, (3) a means for sealed mounting of the vessel-patterned hydrogel membrane to effectively separate the top and bottom chambers and (4) a means of supporting routine culture methods such as frequent media changes. We also incorporated an acrylic grid, directly contacting the underside of the membrane, to provide mechanical stability for the silicone hydrogel, which supports the weight of the cell growth media. To achieve an air- and liquid-tight seal to the membrane, soft silicone rubber (McMaster-Carr, Robbinsville, NJ) gaskets were added to the top and bottom chamber flanges, and the bioreactor assembly was clamped together with thumbscrews. A 9-well adapter insert was fabricated from acrylic for cell culture studies, providing a means for multiplexed experiments. The wells also allowed for spatially separated cultures with smaller surface areas, which helped to prevent Matrigel detachment from the silicone hydrogel membrane.

2.2 Microfabrication of patterned molds

The micropillar designs were generated using AutoCAD software (Autodesk, San Rafael, CA), and written onto chrome-glass photomasks using a DWL66 Laser Writer (*Heidelberg* Instruments Mikrotechnik, Heidelberg, Germany). A template for the micropillars was fabricated using this pattern from a high aspect ratio epoxy based photoresist, SU-8 2150 (MicroChem, Newton, MA). The standard SU-8 patterning process suggested by the manufacturer was used, with minor adjustments to the processing times. Our process was optimized for the specific application of creating high aspect ratio pillars 25–100 μm in diameter and 200–250 μm tall.

The silicon wafer substrate was cleaned, dehydrated on a 200 °C hotplate (20 min), and then treated with MCC Primer 80/20 (MicroChem, Newton, MA) using a spin coater (Model WS-650S-8NPP/LITE, Laurell Technologies, North Wales, PA). For each inch (25 mm) of

substrate diameter, 1 mL of SU-8 2150 resist was dispensed onto the wafer before spinning at 2000 rpm, resulting in a film thickness of 200 – 250 μm. The photoresist edge bead was removed with a swab in order to improve contact with the photomask. After a softbake on leveled hotplates at 65 °C (10 minutes) and 95 °C (70 minutes), the SU-8 coated substrate was brought into vacuum contact with the photomask in the mask aligner (Model 208, Optical Associates, Inc., San Jose, CA). A long pass filter, PL-360-LP (Omega Optical, Brattleboro, VT) was used during the initial exposure of 700 mJ/cm^2 to eliminate UV radiation below 350 nm, thereby minimizing attenuation and scattering through the thickness of the resist to help achieve vertical pillar sidewalls. A second dose of 150 mJ/cm^2 without the filter ensured adequate crosslinking. A post-exposure bake of 5 minutes at 65 °C and 25 min at 95 °C drove the cross-linking reaction to completion, after which the templates were immersed in SU-8 Developer (MicroChem, Newton, MA) for 20–25 min with slight manual agitation. After development, the surface was rinsed thoroughly with isopropanol, dried, and hard baked at 200 °C for 25 min to further cross-link the patterned structures and to promote resist adhesion to the substrate. The completed SU-8 micropillar array was then silanized for 1–2 h by vapor deposition of tridecafluoro-1,1,2,2-tetrahydrooctyl trichlorosilane (Gelest, Morrisville PA). In order to generate the hydrogel micropillars, we needed to make a microwell mold from the SU-8 master. We found that PDMS released well from the SU-8, was compatible with hydrogel casting, and was useful for demolding because of its flexibility, thereby reducing micropillar shearing. To create the negative PDMS mold, the Sylgard® 184 Silicone Elastomer kit (Robert McKeown Co., Branchburg, NJ) base and curing agent were mixed in a 10:1 ratio by weight, cast on the SU-8 master, de-gassed in a vacuum chamber, and baked for 90 min at 80 °C.

2.3 Silicone hydrogel fabrication

Silicone hydrogels were photopolymerized utilizing methacrylate chemistry[36], and were composed of 3-methacryloxypropyltris (trimethylsiloxy) silane (TRIS) monomer (Silar Labs, Wilmington, NC), methacryloxypropyl terminated PDMS (ma-PDMS) macromer (Gelest, Morrisville, PA), *N,N*'-dimethylacrylamide (DMA) monomer (Sigma, St. Louis, MO), *N*-vinyl-2-pyrrolidone (NVP) monomer (Sigma, St. Louis, MO), ethylene glycol dimethacrylate (EGDMA) crosslinking agent, and Irgacure 2100 UV photoinitiator (BASF, Ludwigshafen, Germany). DMA (1 mL), TRIS (4 mL), ma-PDMS (1 mL), NVP (0.36 mL), EGDMA (0.05mL), and Irgacure 2100 (0.051mL) were thoroughly mixed in a glass vial by sonicating (3 × 30 s) in a Branson 1510 ultrasonic water bath (Emerson Industrial Automation, St. Louis, MO) located in a fume hood. This mixture was then poured onto the PDMS mold clamped in an acrylic ring used to contain the mixture. The hydrogel mixture was photopolymerized by exposure to high intensity UV-C for 10–15 min and allowed to outgas overnight. Heating the assembly for 10 min at 80°C facilitated separation of the hydrogel and PDMS mold, and reduced shearing of the delicate micropillar structures. To remove any uncrosslinked material, the silicone hydrogel was rinsed in acetone, followed by a 24 h wash in ethanol on a Roto Mix 50800 orbital shaker (Barnstead Thermolyne, Dubuque, IA).

2.4 Oxygen gradient measurements in bioreactor

To characterize oxygen transport in the bioreactor, and particularly the permeability of the silicone hydrogel, we measured the dissolved O_2 concentration in the bioreactor as a function of distance from a flat silicone hydrogel membrane without cells. For these experiments, we prepared the bioreactor with 0.3% Bacto™ Agar (BD, Franklin Lakes, NJ), in place of the Matrigel used in the cell culture experiments, to a depth of 1 mm above a flat silicone hydrogel membrane, and covered this agar layer with 15 mm of water, instead of culture media, in order to minimize any biological contamination that might skew the oxygen measurements. To measure dissolved O_2 tension as a function of distance from the

hydrogel membrane, we used a 500 μm diameter fiber-optic O_2 sensor probe (FOSPHOR AL300, SpectrEcology, Jasper, GA) with the NeoFox® phase measurement system (OceanOptics, Dunedin, FL), and a custom interface written in LabView (National Instruments Corp., Austin, TX) to acquire the sensor data. Before the start of each measurement, both bioreactor chambers were flooded with 100% N_2 for several hours, until the sensor measured zero oxygen concentration. Upon introduction of 21% O_2 into the lower bioreactor chamber, the dissolved O_2 concentration was measured as a function of time at a number of different heights above the silicone hydrogel membrane, with the resulting steady-state values used to extract a gradient profile. The oxygen sensor system was also used for a separate measurement of the time-dependent oxygen concentration in the bottom chamber for use in the finite element modeling.

2.5 Mathematical modeling of oxygen gradients surrounding vessel mimetics

Finite element modeling of convective flow and oxygen transport in the bioreactor system was performed using COMSOL Multiphysics (Burlington, MA). First, a two-dimensional axisymmetric model of the full bioreactor was used to get a reasonable approximation of the convective flow field generated by the thermal gradients that arise from gas delivery and evaporative cooling. This convective flow field was then used together with the measured oxygen source concentration to calculate the development of the oxygen gradient in the bioreactor without cells. Parametric sweeps of the relative oxygen solubility and diffusion coefficient in the silicone hydrogel were used to find best matches for the experimental data on the time-dependent oxygen concentration immediately above the silicone hydrogel surface. The thermal properties of the silicone hydrogel were assumed to mimic acrylic. Other physical constants were obtained from the literature.

With these parameters set, we switched to a model with a smaller cell and rectangular symmetry in order to be able to include a square array of 50 μm diameter cylindrical pillars in a computationally tractable form. This required the use of an artificially imposed convective field, which we adjusted by choosing vertical flow velocities similar to those found in the full bioreactor calculation and performing parametric sweeps in a 2-D model, with periodic boundary conditions on the edges, to match the oxygen gradient development found in the experimental system and in the full bioreactor computation. Finally, we switched again, this time to a 3-D model that included a square microarray of pillars, using periodic boundary conditions and the 2-D convective flow field found in the earlier calculation with a rectangular cell. After verifying that the time-dependent oxygen gradients were essentially unchanged in this 3-D model, we included the effects of oxygen consumption in the cell-bearing layer, based on typical values found in the literature, in order to provide numerical estimates of the steady-state oxygen gradients experienced by the cell clusters.

2.6 Cell culture in the bioreactor

OVCAR8 human ovarian carcinoma cells and the drug-resistant sub-line NCI/ADR-Res, stably transfected with dsRed2 and EGFP [39], respectively, were chosen for initial evaluation of the bioreactor. Matrigel (BD Biosciences, San Jose, CA) basement membrane extract (BME) was thawed at 4°C overnight. A total volume of 2 mL of the Matrigel-cell mixture, corresponding to a depth of 1 mm, was placed on top of the pillared hydrogel membrane, and allowed to gel at 37 °C. RPMI 1640 medium (Invitrogen) supplemented with 10% fetal bovine serum (HyClone, Logan, UT), penicillin, streptomycin, and L-glutamine (Invitrogen) was added to the top of the BME cultures in the bioreactor to a depth of 14.8 mm (30 mL volume), and was changed every 2 d. The bottom gas chamber of the bioreactor was maintained at a partial pressure of 3% O_2 or 8% O_2, with 5% CO_2, and N_2

constituting the remaining gas. The top chamber mixed-gas source was maintained at 95% N_2 and 5% CO_2. The cultured cells were imaged after 7 d using fluorescence microscopy.

2.7 Matrigel growth controls and image-based quantization

OVCAR8-dsRed2 cells were embedded in media-diluted BD Matrigel (3 mg/mL) at 6×10^5 cells/mL on 8-well μ-slides (Ibidi Gmbh, Munchen, Germany) at 250 μL per well. Each control was grown for 7 d at 3% O_2, 8% O_2 or 21% O_2. Cells were imaged using Axiovision software (Carl Zeiss Microscopy, LLC, Thornwood, NJ). For each pO_2 condition, at least 50 spheroids were imaged and their diameters measured using ImageJ Software (NIH, Bethesda, MD), after using images of a length standard to calibrate the pixel dimensions. The diameter of a tumor spheroid was defined as the average length of its greatest dimension passing through the centroid. For size analysis of spheroids cultured with micropillars in the bioreactor, the diameters of the silicone hydrogel pillars were subtracted from the average spheroid diameter before comparison with control spheroids.

To optimize the baseline culture conditions, we seeded increasing numbers of cells (1.5×10^5, 3.0×10^5, 6.0×10^5, 1.2×10^6, 2.4×10^6, and 4.8×10^6 cells/mL) in increasing concentrations of Matrigel (1.125, 2.25, 4.5, and 9 mg/mL). The largest multicellular clusters were observed for Matrigel concentrations between 2.25 and 4.5 mg/mL.

2.8 Calculation of oxygen gradient within spheroids

Pimonidazole HCl (Hypoxyprobe, Inc., Burlington, MA) is a hypoxia marker, forming adducts to thiol groups selectively in the absence of oxygen (hypoxic cells). We utilized it to determine the extent of hypoxia within our tumor spheroids. Pimonidazole HCl was added to the culture media under various growth conditions at a final concentration of 100 μg/mL and allowed to incubate for 2 h. The spheroids were then isolated using a micropipette tip guided by microscopic visualization, fixed in 4% paraformaldehyde for 24 h, embedded in low melting point paraffin wax (Electron Microscopy Science, Inc., Hatfield, PA), and sectioned. After antigen retrieval, sections were stained with Mouse Anti-Pimonidazole Monoclonal Antibody (Hypoxyprobe, Inc., Burlington, MA) at a concentration of 1:100. Anti-mouse HRP secondary antibody was used. In order to quantify hypoxic gradients within individual spheroids, an image processing script was written in MATLAB (Mathworks, Inc., Natick, MA) to spectrally isolate the brown staining and generate a grayscale image. The resultant image was sectioned concentrically and pixel intensities were summed (n=3). Data was reported as a percentage of maximal staining intensity vs. distance from the center of the spheroid. Prediction bounds were computed using MATLAB's curve fitting toolbox.

3. Results

3.1 Bioreactor design and fabrication

A bioreactor system was necessary for mounting the micro-patterned silicone hydrogel (SiHy) membrane between two sealed chambers, enabling pillar-induced O_2 tension in the Matrigel culture. The system's 3-D CAD design is shown in Fig. 1B: the SiHy membrane is clamped between the oxygenated (bottom) and the anoxic (top) controlled chamber, consistent with the experimental cell growth model shown in Fig. 1A. An acrylic support grid (1 cm spacing, <1 mm bar width) (Fig. 1B) contacts the bottom surface of the membrane to assist in supporting the weight of growth media, minimizing the potential for membrane mechanical failure. The fully assembled bioreactor is approximately 17 cm in height and 10 cm in diameter at its widest. A sensor-regulated acrylic hypoxia enclosure (BioSpherix, Ltd., Lacona, NY) was used for precise, continuous control of O_2 tension in the bottom chamber of the bioreactor during our cell culture experiments and was fed by

modified gas ports that extended outside the incubator to in-line gas flowmeters (Key Instruments, Trevose, PA).

3.2 Micropatterned SiHy membrane preparation

The aim of this study was to create an oxygen-permeable hydrogel membrane with integrated high aspect ratio micropillars to mimic O_2 perfusion from capillaries for growth of cancer cells in basement membrane extract (i.e., Matrigel). After the construction of the bioreactor, a process was developed to produce vessel mimetics via microfabrication methods. A soft lithography technique for forming silicone hydrogel micropillars was developed and is shown in Fig. 2. Photolithographic designs were created for pillar diameters ranging from 15 μm to 100 μm. The pillars were arranged in 100 × 100 arrays covering a total physical area of 5 mm by 5 mm. Each hydrogel membrane included several separate arrays of pillars with different diameters to enable simultaneous evaluation of various pillar sizes, and was later revised to create membranes with 50 μm or 100 μm diameter pillars, exclusively. Initial fabrication attempts using a single-step process in which we cast silicone hydrogel into SU-8 microwells failed due to adhesion of the hydrogel to the photoresist, photoresist cracking, and poor pillar feature replication. Consequently, we then developed a two-step process starting with positive features in SU-8 (Fig. 2A – C), followed by a negative mold in PDMS (Fig. 2-D–E), upon which silicone hydrogel was cast, crosslinked and demolded (Fig. 2F –G).

Scanning electron microscope (SEM) images depict the results of the fabrication process: SU-8 master (Fig. 3A, created in step C of Fig. 1), PDMS mold (Fig. 2B, created after step E in Fig. 2), and final silicone hydrogel micropillar membrane (Fig. 3C–F, resulting from step G in Fig. 2). The 15 μm diameter micropillars were extremely fragile and typically collapsed, whereas diameters of 25 μm, 50 μm and 100 μm were successfully fabricated. The heights of the final membrane micropillars ranged from 200 to 275 μm (Fig. 3C – F), corresponding to aspect ratios of up to 7.5 (Fig. 3, E). The most challenging aspect of fabrication was minimizing pillar tearing during the demolding process, both at the flat membrane junction and along the length of the pillar itself. The silicone hydrogel formation was chosen to provide sufficient shear modulus to enable demolding. Because of the two-step PDMS-hydrogel molding process, varying pillar vertical wall angles is not an option. Therefore, various solvents (e.g., toluene, acetone) known to swell PDMS [40] were tested as release agents during demolding and helped to reduce the rate of pillar shearing. Best results were obtained by using acetone as a release aid.

3.3 O_2 permeability of SiHy

Because different silicone hydrogel formulations vary in their diffusivity of O_2 [36], we empirically determined O_2 diffusion through our formulation in the dual-chamber bioreactor system using a micro-O_2 probe. A flat hydrogel membrane was mounted in the bioreactor system, between the bottom chamber, with input gas of ~21% O_2, and the top chamber, with continuously flowing 95% N_2 gas (~57 SCCM) and 5% CO_2 gas (~3 SCCM) (Fig. 1B). Although we explored the use of a motor-actuated stage to measure the steady-state O_2 gradient, in the end we focused on time-dependent measurements at fixed sensor positions, out of concern that any sensor movement might disrupt the convective flow cells in the bioreactor.

From the measurements of O_2 equilibration at different vertical positions in the bioreactor, we constructed a steady-state gradient profile (Fig. 4A). The O_2 tension is saturated near the silicone hydrogel surface, and falls off sharply in the agar layer where diffusion is the dominant mode of transport. The O_2 concentration in the water above the agar is non-zero and roughly constant as a function of height, likely due to convective mixing in the fluid and

limitations in mass transfer across the water-gas boundary at the top surface. The equilibration curves (Fig. S2) show minor run-to-run variations that could easily arise from slight variations in the initial system temperatures and gas flow rates. However, the equilibrium values and resultant steady-state O_2 gradients are more consistent. It should be noted that in our cell culture experiments with gas input of < 8% O_2, this gradient would pervade a considerably smaller range.

In order to get a better understanding of the overall O_2 transport in this system, we constructed a finite element model of the full bioreactor volume and calculated the expected fluid convection, using input gas temperatures of 34 °C in an incubator maintained at 37 °C. As seen in Fig. S1A, the convective flow was predominantly down in the center of the bioreactor and up at the walls, with maximum velocities on the order of 700 μm/s at the center. Using 3×10^{-9} m^2/s for the diffusion coefficient of O_2 in water at 37 °C [41] and 7×10^{-6} m/s for the O_2 mass transfer coefficient across the interface between the 37 °C water and the anoxic gas [42], we performed parametric sweeps of the O_2 diffusion coefficient in the silicone hydrogel and the partition coefficient (ratio of O_2 solubilities) between the silicone hydrogel and the agarose. From comparing the results of these sweeps with the experimental data for O_2 equilibration immediately above the silicone hydrogel surface (data not shown), we obtained estimates of the O_2 diffusion coefficient in the silicone hydrogel (5×10^{-9} m^2/s), and the partition coefficient (8) that were in reasonable agreement with numbers found in the literature for similar materials (PDMS) [43]. Using these parameters in the finite element model, we then calculated the steady state O_2 distribution in the full bioreactor (Fig. S1B), from which we extracted the steady-state oxygen concentration as a position of distance from the SiHy membrane, averaged over a 500 μm diameter area at the center of the bioreactor at each height (Fig. 4B). Given that the simulation essentially has no freely determined parameters, the agreement between the experimental data and the calculation is reasonably good, particularly taking into account known uncertainties in the sensor position. For further verification, we also calculated the full time-dependent O_2 concentration in the bioreactor at heights corresponding to those used in the oxygen measurements (Fig. S2B), and also found reasonable agreement with the experimental data (Fig. S2A).

3.4 Modeling of O_2 gradient around SiHy micropillars

Using the convective flow velocities from the computational model and the O_2 equilibration measurements as a guide, we constructed a finite element model for a square segment of the bioreactor, in order to be able to calculate the detailed O_2 concentration around the micropillars. After finding an artificial convective transport field for this smaller cell that produced O_2 concentrations matching both the experimental data and the computation for the full bioreactor, we modeled the effects of O_2 consumption by assuming uniform cell density in the full Matrigel layer. We followed previously reported models for O_2 consumption in close-packed cells [44–46], which use a Michaelis-Menten form:

$$Rate\ of\ O_2 consumption = R_{max} \frac{c_{O_2}}{c_{O_2} + C_{MM}}$$

where R_{max} is the maximum rate of O_2 consumption, and C_{MM} is the Michaelis-Menten constant. We assumed the Matrigel layer to be uniformly filled with close packed cells, and used two sets of values found for flask-based culture of EMT6/Ro cells, R_{max} = 0.014 and 0.028 mol/m^3-s and $C_{MM} = 2 \times 10^{-3}$ and 7×10^{-3} $moles/m^3$, respectively [45]. The initial O_2 concentration was set to zero everywhere. We set the source O_2 concentration at the top surface of the silicone hydrogel to either 32 μM or 84 μM, found by using Henry's law to

calculate the concentration of O_2 water in equilibrium with 3% or 8% O_2 at 37 °C. As a result, these calculations do not include longitudinal concentration gradients along the pillars; from checks made with a single isolated pillar in a 2-D axisymmetric model, we estimate that the O_2 concentration at the top of the pillar is in fact approximately 10% lower than at the bottom. In addition, we found that convective flow in the media has minimal effect on the O_2 concentration for these consumption parameters, under the simplifying if unrealistic assumption that the Matrigel volume is completely filled with cells, and so we omitted convective flow from the calculations that include consumption. Including the convective mixing would become necessary if the actual distribution of cells through a relatively small fraction the Matrigel were taken into account, or if the cellular O_2 consumption is lower than we assume here. However, a more sophisticated model that would include the growth of spatially heterogeneous cell clusters is beyond the scope of this present work, which focuses on assessing the potential utility of the bioreactor rather than on understanding cell cluster growth.

The results of the 3-D bioreactor calculations are shown in Figure 5. The equilibrium O_2 gradient for a vertical plane transecting the pillars in the absence of cellular O_2 consumption (Fig.5A) is considerably different from that seen with cells present (Figs 5C–F). When O_2 consumption is included in the calculations, the O_2 concentration falls off sharply away from the pillars, leading to well-defined gradients in the interstitial spaces for all the conditions considered (Figs. 5B–E). As expected, the gradients are more pronounced for the higher consumption rates (Figs. 5D and F, with R_{max} = 0.028 mol/m^3-s and C_{MM} =7 × 10^{-3} moles/m^3), but still sufficient to govern the spatial distribution of cells for the lower consumption rate considered (Figs. 5C and E, with R_{max} = 0.014 mol/m^3-s and C_{MM} =2 × 10^{-3} moles/$m^{3)}$. In addition, the shape of the gradient varies with the source O_2 concentration, with a 3% O_2 source (Figs. 5C and D) leading to a more rapid decrease in away from the pillars than is seen for the 8% O_2 source (Figs. 5E and F), even after rescaling.

3.5 Assessment of 3-D culture in bioreactor

In vivo, tumors often consist of many small clusters of cells around a capillary, with cells no more than 100 μm away from the nearest blood vessel [35, 47]. For the microfabricated artificial vessel system, our goal was to mimic the geometric distribution of capillaries to provide similar O_2 diffusion and distribution, thereby enabling growth of similar cell aggregates.

For our initial culture experiments, a SiHy membrane patterned with micropillars (25, 50 or 100 μm diameter) spaced 200 μm apart on-center was loaded in the dual-chamber bioreactor. OVCAR8 human ovarian carcinoma cells, stably transfected with dsRed2 red fluorescent protein to facilitate visualization of cells, were suspended in 2 mL of diluted Matrigel (3 mg/mL) and deposited on the polymeric vessel substrate at a density of 6 × 10^5 cells/mL. After depositing the cell-Matrigel suspension on the pillared hydrogel membrane, allowing the Matrigel to gel, and partially filling the top chamber with media, the bioreactor is sealed (i.e., top lid via thumbscrews) and placed in the hypoxia chamber within the incubator. The gas mixture input to the top chamber was 95% N_2 and 5% CO_2. The input gas source in the bottom chamber was set at atmospheric pressure with 3% O_2 or 8% O_2, corresponding to 39 mm Hg and 103 mm Hg, respectively, after adjusting for the difference in solubility between N_2 and O_2 in water. These O_2 tensions are not used for conventional cell culture (21% O_2 or 271 mm Hg), but instead correspond to *in vivo* arterial and venous blood O_2 at roughly 75 – 100 mm Hg and 40 – 50 mm Hg, respectively [48]. After 7 d growth, both confocal and light microscopy were used to image the cultures (Fig. 6). Hoechst staining of nuclear DNA was used to better visualize cell density. With the bottom chamber at 3% and 8% O_2 tension (top, left and center panels), the 3-D cell cultures in the bioreactor showed altered growth

patterns, surrounding the pillars with spheroid-like morphology and larger clusters than seen for parallel cultures in Matrigel-filled wells (bottom, left and center panels). In some instances, the multicellular clusters were observed growing up and around the length of the pillars. Cells were observed growing as far away as 100 μm radially from the pillars, which is similar to reports on *in vivo* distribution of cells surrounding vessels [35, 47, 49]. In addition to forming large multicellular spheroids around and between the pillars, the OVCAR8-dsRed2 cells were able to adhere to the SiHy membrane base to form a monolayer.

Control experiments in the bioreactor were performed to confirm that the observed growth patterns were a result of the O_2 delivery via micropillars, rather than the structural or adhesion support provided by the micropillars (Fig. 6, right panel). OVCAR8-dsRed2 cells were cultured in the bioreactor in the absence of an O_2 gradient with a 3% O_2 concentration in both the top and bottom bioreactor chambers (top, right panel). As anticipated, without the O_2 gradient, the cells formed smaller multicellular spheroids throughout the Matrigel rather than extended structures around the micropillars (outlined in white). The bioreactor culture without an O_2 gradient strongly resembles the 3-D control cultures in Matrigel (bottom, left and center panels). A second bioreactor control with an input gas gradient of 3% O_2 and no SiHy micropillars showed similar results (bottom, right panel). Together, these results suggest that the extended growth morphology seen for OVCAR8-dsRed cells in the bioreactor is caused by O_2 diffusion through the micropillars.

Additional bioreactor experiments involved using a different membrane material or co-culturing two ovarian epithelial cell types. PDMS was investigated for potential use as an alternative to SiHy with this system by incorporating a PDMS micropillar membrane into the same bioreactor set-up with 3% oxygen in the bottom chamber. Results showed similar MCTS growth around (Fig. S3A) and branching between the micropillar structures (Fig. S3B–E). Co-culture experiments in the bioreactor with OVCAR8-dsRed2 (red) and NCI/ADR-Res EGFP (green) fluorescent cell lines also showed large cluster formation surrounding SiHy micropillars (Fig. S4), with both drug-sensitive and drug-resistant cell lines growing together in clusters.

3.6 Comparison of bioreactor growth characteristics with MCTS

The tumor microenvironment is characterized by gradients in hypoxia, acidity, and the rate of cell proliferation, all of which can influence tumor growth and drug sensitivity [49]. The oxygenation and proliferation status of cultured OVCAR8-dsRed2 cells in the bioreactor were compared to that of spheroids grown in Matrigel-filled microwells at different O_2 concentrations (Fig. 7). Ki67 and Hypoxyprobe (pimonidazole hydrochloride) histochemical staining were performed to observe the relative extent of cell proliferation and hypoxia, respectively. Culture samples from a bioreactor gradient experiment with the bottom chamber fixed at 8% O_2 contain large cellular aggregates still proliferating after 7 d (Fig. 7, top panels).

Standard MCTS cultures (Fig. 7, lower six panels) were grown in Matrigel-filled microwells for 7 d at three different oxygen concentrations: 3% O_2, 8% O_2 and 21% O_2. As might be expected, cell proliferation (indicated by Ki67 staining) increased with O_2 tension and cellular hypoxia (indicated by PIM staining) decreased (Fig. 7). The images suggest that standard MCTS cell culture at 21% O_2 inadequately models hypoxic conditions found *in vivo*, as all the OVCAR8-dsRed2 cells appear to be proliferative with minimal levels of hypoxia. The considerable cellular proliferation rate and reduced hypoxia staining seen in the bioreactor cultures indicate that an O_2 tension of 8% (103 mm Hg) is sufficient for sustaining cell growth, but could be lowered to 3% (39 mm Hg) to increase the hypoxia gradient while maintaining similar cell cluster sizes.

From image-based analysis of a minimum of 50 spheroids per culture condition, we found that MCTSs grown in the standard Matrigel control cultures are approximately 70% smaller in diameter than the clusters grown in the bioreactor (Fig. S5). The standard MCTS control cultures showed little difference in cell growth at 3% and 21% O_2 tension, as measured by spheroid cluster diameter. Regardless of O_2 tension, spheroid size was observed to be limited to 50 – 70 μm in previously optimized Matrigel conditions. Using silicone hydrogel micropillars to control and perfuse O_2 into 3-D culture resulted in larger cell clusters around the artificial vessels compared to standard MCTS culture in Matrigel (Fig. S5). The 3-D bioreactor cultures showed no difference in average cluster size at 3% and 8% O_2 tension, but were comparatively larger (185 – 200 μm) than the MCTS control cultures in Matrigel-filled microwells. Mean cell cluster size in Matrigel without oxygen diffusing micropillars was 50 μm, whereas with artificial vessels the mean cell cluster size was 183 μm, $p=0.001$. In addition to the size differences, we showed oxygen tension gradients inside the spheroid clusters oxygenated by polymer vessel mimetics had a 100-μm drop-off to hypoxia (Fig. 8C), which is consistent with *in vivo* studies.

3.7 O_2 gradients within tumor organoids

It is widely accepted that O_2 tension is insufficient to support cells in normal tissues more than ~100 μm away from a capillary, resulting in diffusion-limited hypoxia in tumors [50]. This results in a chord-like organization, with tumor nodules arranged cylindrically along the length of a capillary [47]. To assess whether this vessel-localized morphology was replicated in our bioreactor culture, tumor organoids grown in the bioreactor with the bottom chamber fixed at 3% O_2 were harvested and stained with Hypoxyprobe-1 (pimonidazole hydrochloride) for comparison with gradients found in similar studies involving *in vivo* tumors. A representative tumor organoid, a stained section of which is seen in Fig. 8A, was removed under the microscope from a micropillar. The location where the micropillar passed through the organoid (circled) conceivably prevented central hypoxia, despite the 3% O_2 concentration in the bottom chamber to 3% O_2.The intensity of pimonidazole staining appears to increase with distance from the micropillar (Fig. 8A), suggesting a radial hypoxia gradient. This gradient is better visualized using phase enhancement as seen in Fig. 8B, and is further represented by plotting stain intensity as a function of distance from the SiHy micropillar in Fig. 8C. This hypoxia gradient is the inverse of what is seen in a typical MCTS, for which hypoxia increases inward towards a necrotic, anoxic core.

4. Discussion

Capturing the complex features of the *in vivo* tumor microenvironment *in vitro* has become increasingly important to create realistic tumor models aimed at advancing cancer research and drug discovery. While conventional 3-D culture systems offer an advantage over monolayer culture, oxygenation of 3-D cultures does not follow the logic of *in vivo* oxygenation. Here we utilized a 3-D bioreactor culture system with O_2-permeable polymers to create vessel mimetics for that end (Fig. 1). A soft lithography process was established using intermediate PDMS molds (Fig. 2) to achieve oxygen-permeable SiHy substrates with micropatterned pillars (Fig. 3). Micropatterned SiHy membranes demonstrated an effective platform for controllable O_2 delivery (Figs. 4, 5) to cancer cells in 3-D culture (Fig. 8), mimicking *in vivo* O_2 diffusion from vasculature.

Previous efforts to control O_2 delivery to multicellular spheroids have relied on two general approaches, the first aimed at minimizing central nutrient deficiency by controlling spheroid dimension, and the second aimed at simulating artificial vascular circulation. The emerging fields of microfabrication and microfluidics provide powerful tools for guiding cell culture and creating microscale flows to support both of these goals. Multiple studies have reported the use of microfabricated structures to control and optimize the size and geometry of 3-D

cultures in order to better mimic *in vivo* growth [22, 25, 27, 51]. Microwells have been used to guide multicellular self-assembly for generation of uniform multicellular spheroids while microchannels have been used to simulate vascular circulation in engineered tissue, albeit with the distances between vessels much larger than typical intercapillary spacings [12, 25, 27]. Microfluidic device systems incorporating hydrogels have also been described for tissue engineering and drug delivery systems [52, 53].

Another approach, which was applied in the current study, aims to more faithfully replicate physiologic oxygenation of cells. In order to more faithfully replicate *in vivo* conditions, oxygen carriers such as fluorocarbon or liposome-encapsulated hemoglobin have previously been employed [54, 55]. Methodologies more similar to this study have focused on the use of oxygen-permeable membranes to oxygenate multicellular spheroid culture systems [43, 56– 59], including approaches such as using gas-permeable PDMS arrays to provide direct, continuous oxygenation of human hepatoma (HepG2) spheroids [56], demonstrating a reduction in central hypoxia. Similar work by Evenou *et al.* [58, 59] used PDMS membranes to culture hepatocytes with 3-D micropillar structures in order to address the issue of growth-limiting hypoxia in multilayer cell culture. However, their system was primarily designed to increase substrate surface area and oxygenation in a uniform gas environment of 21% O_2 rather than to re-create tumor hypoxia gradients as described here.

Many bioreactor systems, including rotating wall vessels, hollow-fiber and perfusion systems, have previously been developed to increase mass transport of nutrients and oxygen in cell culture [34, 60–62]. Hollow-fiber bioreactors culture cells: (1) within hollow fibers surrounded by media [63, 64] or (2) outside hollow-fiber polymer networks that act as artificial capillaries [65–68]. Akin to *in vitro* multicellular tumor spheroid (MCTS) culture, 3D hollow-fiber models display significantly higher drug resistance compared to conventional cell culture [64], making them promising candidates for anti-cancer therapy studies.

However, perfusion systems such as these often require large amounts of media, limiting their efficiency in drug screening applications that seek to minimize the expense of drug testing. Bettahalli *et al.* [65] integrated hollow-fiber membranes and biodegradable copolymer scaffolds to overcome diffusion limitations in 3-D culture. Our method involves a similar philosophy of engineering artificial microvasculature, but on a smaller scale with greater focus on providing physiologic O_2 gradients via internal oxygenation at length scales which mimic the *in vivo* environment. A key advantage of this approach is that it provides vessel analogs with tunable, uniform spacing. These advantages could lead to implementations aimed at scalability and compatibility with up- and down-stream processes and instrumentation (e.g., high-throughput imaging and analysis).

Rather than focusing on simply increasing the overall O_2 transport to cells in 3-D culture, as in these previously described methods, our system aimed to provide *in vivo*-like O_2 distribution and gradients. Our method of oxygenating MCTSs centrally through artificial polymeric micropillars is distinct from previous approaches. The use of micropillars achieved growth morphologies centered around the oxygen source, and compact geometries that were larger than conventional MCTS controls in Matrigel. Without vascularization, current 3-D culture methods suffer from the inverse logic of oxygenation and remain largely limited to modeling avascular tumors and micrometastases. The bioreactor system described here has potential advantages for developing vascular epithelial tumor models by oxygenating spheroid-forming epithelial cancer cells via polymer vessel mimetics. To the best of our knowledge, the case of *in vivo* epithelial cancer vascular solid tumors has not previously been modeled *in vitro*, but holds significant clinical relevance for cancer research and drug development studies.

Our preliminary results demonstrate that O_2 diffusion through SiHy micropillars reverses the characteristic hypoxia gradients seen in standard MCTS culture. Hypoxia gradient staining (Figs. 7–8) revealed that the tumor spheroid models created using this culture system were more characteristic of vascularized tumors *in vivo*, compared to current MCTS models. As we hypothesized, tumors oxygenated by our synthetic vessels reached maximum pimonidazole staining intensity ~100 μm away from the surface of the synthetic vessel, corresponding to the midpoint between adjacent pillars. We were unable to make a direct comparison with control MCTSs because they did not grow to similar sizes.

Despite this system's potential to facilitate future cancer studies, it is an early model—a proof-of-concept that is not without limitations. The conceptual development of the model led to many design considerations and challenges. Now that the foundation has been laid, we seek to build upon these promising results with additional experiments on a larger scale. This will involve continued optimization of the membrane material and testing of other human epithelial carcinoma cell lines, as well as primary human cancers within the bioreactor system. Future work will modify the bioreactor and micropillar membrane designs to enable larger scale multi-well cultures for higher-throughput studies, while simplifying operation and maintenance.

5. Conclusions

This study reports the development of a 3-D cell culture system to facilitate gas exchange and create oxygen gradients that reflect the tumor microenvironment. Oxygen-permeable polymer micropillars were developed as vessel mimetics to facilitate O_2 delivery to surrounding cancer cell organotypic cultures in anoxia. This work has obvious implications for improving *in vitro* tumor models aimed at assessing new cancer therapies or studying mechanisms of clinical drug resistance, but also holds potential for aiding the growth of large tissue constructs.

Supplementary Material

Refer to Web version on PubMed Central for supplementary material.

Acknowledgments

This work was supported by the Intramural Research Program of the NIH, the National Cancer Institute, the Center for Information Technology, and the National Institute of Biomedical Imaging and Bioengineering.

References

1. Elsdale T, Bard J. Collagen substrata for studies on cell behavior. J Cell Biol. 1972; 54:626–637. [PubMed: 4339818]
2. Pampaloni F, Reynaud EG, Stelzer EHK. The third dimension bridges the gap between cell culture and live tissue. Nat Rev Mol Cell Bio. 2007; 8:839–845. [PubMed: 17684528]
3. Debnath J, Brugge JS. Modelling glandular epithelial cancers in three-dimensional cultures. Nat Rev Cancer. 2005; 5:675–688. [PubMed: 16148884]
4. Weigelt B, Bissell MJ. Unraveling the microenvironmental influences on the normal mammary gland and breast cancer. Semin Cancer Biol. 2008; 18:311–321. [PubMed: 18455428]
5. Gillet JP, Calcagno AM, Varma S, Marino M, Green LJ, Vora MI, et al. Redefining the relevance of established cancer cell lines to the study of mechanisms of clinical anti-cancer drug resistance. Proc Natl Acad Sci U S A. 2011; 108:18708–18713. [PubMed: 22068913]
6. Zhang S. Beyond the Petri dish. Nat Biotechnol. 2004; 22:151–152. [PubMed: 14755282]

7. Mehta JP, O'Driscoll L, Barron N, Clynes M, Doolan P. A microarray approach to translational medicine in breast cancer: how representative are cell line models of clinical conditions? Anticancer Res. 2007; 27:1295–1300. [PubMed: 17593622]
8. Gillet JP, Varma S, Gottesman MM. The Clinical Relevance of Cancer Cell Lines. J Natl Cancer I. 2013; 105:452–458.
9. Yamada KM, Cukierman E. Modeling tissue morphogenesis and cancer in 3D. Cell. 2007; 130:601–610. [PubMed: 17719539]
10. Hanahan D, Coussens LM. Accessories to the crime: functions of cells recruited to the tumor microenvironment. Cancer Cell. 2012; 21:309–322. [PubMed: 22439926]
11. Fischbach C, Chen R, Matsumoto T, Schmelzle T, Brugge JS, Polverini PJ, et al. Engineering tumors with 3D scaffolds. Nat Methods. 2007; 4:855–860. [PubMed: 17767164]
12. Griffith LG, Swartz MA. Capturing complex 3D tissue physiology in vitro. Nat Rev Mol Cell Biol. 2006; 7:211–224. [PubMed: 16496023]
13. Kenny PA, Lee GY, Myers CA, Neve RM, Semeiks JR, Spellman PT, et al. The morphologies of breast cancer cell lines in three-dimensional assays correlate with their profiles of gene expression. Mol Oncol. 2007; 1:84–96. [PubMed: 18516279]
14. Bissell MJ, Hall HG, Parry G. How Does the Extracellular-Matrix Direct Gene-Expression. J Theor Biol. 1982; 99:31–68. [PubMed: 6892044]
15. Nelson CM, Bissell MJ. Of extracellular matrix, scaffolds, and signaling: tissue architecture regulates development, homeostasis, and cancer. Ann Rev Cell Dev Biol. 2006; 22:287–309. [PubMed: 16824016]
16. Kleinman HK, Philp D, Hoffman MP. Role of the extracellular matrix in morphogenesis. Curr Opin Biotechnol. 2003; 14:526–532. [PubMed: 14580584]
17. Weaver VM, Petersen OW, Wang F, Larabell CA, Briand P, Damsky C, et al. Reversion of the malignant phenotype of human breast cells in three-dimensional culture and in vivo by integrin blocking antibodies. J Cell Biol. 1997; 137:231–245. [PubMed: 9105051]
18. Hutmacher DW. Biomaterials offer cancer research the third dimension. Nat Mater. 2010; 9:90–93. [PubMed: 20094076]
19. Hovinga KE, Shimizu F, Wang R, Panagiotakos G, Van Der Heijden M, Moayedpardazi H, et al. Inhibition of notch signaling in glioblastoma targets cancer stem cells via an endothelial cell intermediate. Stem Cells. 2010; 28:1019–1029. [PubMed: 20506127]
20. Stoppini L, Buchs PA, Muller D. A simple method for organotypic cultures of nervous tissue. J Neurosci Methods. 1991; 37:173–182. [PubMed: 1715499]
21. Loessner D, Stok KS, Lutolf MP, Hutmacher DW, Clements JA, Rizzi SC. Bioengineered 3D platform to explore cell-ECM interactions and drug resistance of epithelial ovarian cancer cells. Biomaterials. 2010; 31:8494–8506. [PubMed: 20709389]
22. Loessner D, Flegg JA, Byrne HM, Clements JA, Hutmacher DW. Growth of confined cancer spheroids: a combined experimental and mathematical modelling approach. Integr Biol (Camb). 2013; 5:597–605. [PubMed: 23388834]
23. Miller BE, Miller FR, Heppner GH. Factors affecting growth and drug sensitivity of mouse mammary tumor lines in collagen gel cultures. Cancer Res. 1985; 45:4200–4205. [PubMed: 4028010]
24. Szot CS, Buchanan CF, Freeman JW, Rylander MN. 3D in vitro bioengineered tumors based on collagen I hydrogels. Biomaterials. 2011; 32:7905–7912. [PubMed: 21782234]
25. Lin RZ, Chang HY. Recent advances in three-dimensional multicellular spheroid culture for biomedical research. Biotechnol J. 2008; 3:1172–1184. [PubMed: 18566957]
26. Sutherland RM. Cell and environment interactions in tumor microregions: the multicell spheroid model. Science. 1988; 240:177–184. [PubMed: 2451290]
27. Hirschhaeuser F, Menne H, Dittfeld C, West J, Mueller-Klieser W, Kunz-Schughart LA. Multicellular tumor spheroids: an underestimated tool is catching up again. J Biotechnol. 2010; 148:3–15. [PubMed: 20097238]
28. Serebriiskii I, Castello-Cros R, Lamb A, Golemis EA, Cukierman E. Fibroblast-derived 3D matrix differentially regulates the growth and drug-responsiveness of human cancer cells. Matrix Biol. 2008; 27:573–585. [PubMed: 18411046]

29. Kleinman HK, Martin GR. Matrigel: Basement membrane matrix with biological activity. Semin Cancer Biol. 2005; 15:378–386. [PubMed: 15975825]
30. Benton G, George J, Kleinman HK, Arnaoutova IP. Advancing science and technology via 3D culture on basement membrane matrix. J Cellular Physiol. 2009; 221:18–25. [PubMed: 19492404]
31. Kleinman HK, McGarvey ML, Liotta LA, Robey PG, Tryggvason K, Martin GR. Isolation and characterization of type IV procollagen, laminin, and heparan sulfate proteoglycan from the EHS sarcoma. Biochemistry. 1982; 21:6188–6193. [PubMed: 6217835]
32. Leight JL, Liu WDF, Chaturvedi RR, Chen S, Yang MT, Raghavan S, et al. Manipulation of 3D Cluster Size and Geometry by Release from 2D Micropatterns. Cell Mol Bioeng. 2012; 5:299–306. [PubMed: 23730348]
33. Kunz-Schughart LA. Multicellular tumor spheroids: intermediates between monolayer culture and in vivo tumor. Cell Biol Int. 1999; 23:157–161. [PubMed: 10562436]
34. Friedrich J, Ebner R, Kunz-Schughart LA. Experimental anti-tumor therapy in 3-D: spheroids--old hat or new challenge? Internatl J Radiation Biol. 2007; 83:849–871.
35. Minchinton AI, Tannock IF. Drug penetration in solid tumours. Nat Rev Cancer. 2006; 6:583–592. [PubMed: 16862189]
36. Kim J, Conway A, Chauhan A. Extended delivery of ophthalmic drugs by silicone hydrogel contact lenses. Biomaterials. 2008; 29:2259–2269. [PubMed: 18289662]
37. Lai YC. Novel Polyurethane Silicone Hydrogels. J Appl Polym Sci. 1995; 56:301–310.
38. Nicolson PC, Vogt J. Soft contact lens polymers: an evolution. Biomaterials. 2001; 22:3273–3283. [PubMed: 11700799]
39. Brimacombe KR, Hall MD, Auld DS, Inglese J, Austin CP, Gottesman MM, et al. A dual-fluorescence high-throughput cell line system for probing multidrug resistance. Assay Drug Dev Technol. 2009; 7:233–249. [PubMed: 19548831]
40. Lee JN, Park C, Whitesides GM. Solvent compatibility of poly(dimethylsiloxane)-based microfluidic devices. Anal Chem. 2003; 75:6544–6554. [PubMed: 14640726]
41. St-Denis CE, Fell CJD. Diffusivity of oxygen in water. Can J Chem Eng. 1971; 49 885–.
42. Downing AL, Truesdale GA. Some factors affecting the rate of solution of oxygen in water. J Applied Chem. 1955; 5:570–581.
43. Nishikawa M, Yamamoto T, Kojima N, Kikuo K, Fujii T, Sakai Y. Stable immobilization of rat hepatocytes as hemispheroids onto collagen-conjugated poly-dimethylsiloxane (PDMS) surfaces: Importance of direct oxygenation through PDMS for both formation and function. Biotechnol Bioeng. 2008; 99:1472–1481. [PubMed: 17969156]
44. Buchwald P. FEM-based oxygen consumption and cell viability models for avascular pancreatic islets. Theor Biol Med Model. 2009:6. [PubMed: 19416527]
45. Casciari JJ, Sotirchos SV, Sutherland RM. Variations in tumor cell growth rates and metabolism with oxygen concentration, glucose concentration, and extracellular pH. J Cellular Physiol. 1992; 151:386–394. [PubMed: 1572910]
46. Mehta G, Mehta K, Sud D, Song JW, Bersano-Begey T, Futai N, et al. Quantitative measurement and control of oxygen levels in microfluidic poly(dimethylsiloxane) bioreactors during cell culture. Biomed Microdevices. 2007; 9:123–134. [PubMed: 17160707]
47. Tannock IF. The relation between cell proliferation and the vascular system in a transplanted mouse mammary tumour. Br J Cancer. 1968; 22:258–273. [PubMed: 5660132]
48. L, Goldman; AI, Schafer, editors. Goldman’s Cecil Medicine. 24th ed.. Philadelphia, PA: Elsevier/Saunders; 2012.
49. Tredan O, Galmarini CM, Patel K, Tannock IF. Drug resistance and the solid tumor microenvironment. J Natl Cancer Inst. 2007; 99:1441–1454. [PubMed: 17895480]
50. Thomlinson RH, Gray LH. The Histological Structure of Some Human Lung Cancers and the Possible Implications for Radiotherapy. Brit J Cancer. 1955; 9 539-&.
51. Yoshii Y, Waki A, Yoshida K, Kakezuka A, Kobayashi M, Namiki H, et al. The use of nanoimprinted scaffolds as 3D culture models to facilitate spontaneous tumor cell migration and well-regulated spheroid formation. Biomaterials. 2011; 32:6052–6058. [PubMed: 21640378]

52. Ainslie KM, Kraning CM, Desai TA. Microfabrication of an asymmetric, multi-layered microdevice for controlled release of orally delivered therapeutics. P Soc Photo-Opt Ins. 2008; 8:1042–1047.
53. Geckil H, Xu F, Zhang XH, Moon S, Demirci U. Engineering hydrogels as extracellular matrix mimics. Nanomedicine-Uk. 2010; 5:469–484.
54. Khattak SF, Chin KS, Bhatia SR, Roberts SC. Enhancing oxygen tension and cellular function in alginate cell encapsulation devices through the use of perfluorocarbons. Biotechnol Bioeng. 2007; 96:156–166. [PubMed: 16917927]
55. Nahmias Y, Kramvis Y, Barbe L, Casali M, Berthiaume F, Yarmush ML. A novel formulation of oxygen-carrying matrix enhances liver-specific function of cultured hepatocytes. FASEB J. 2006; 20:2531–2533. [PubMed: 17077286]
56. Anada T, Fukuda J, Sai Y, Suzuki O. An oxygen-permeable spheroid culture system for the prevention of central hypoxia and necrosis of spheroids. Biomaterials. 2012; 33:8430–8441. [PubMed: 22940219]
57. Curcio E, Salerno S, Barbieri G, De Bartolo L, Drioli E, Bader A. Mass transfer and metabolic reactions in hepatocyte spheroids cultured in rotating wall gas-permeable membrane system. Biomaterials. 2007; 28:5487–5497. [PubMed: 17881050]
58. Evenou F, Couderc S, Kim B, Fujii T, Sakai Y. Microfibrillated Cellulose Sheets Coating Oxygen-Permeable PDMS Membranes Induce Rat Hepatocytes 3D Aggregation into Stably-Attached 3D Hemispheroids. J Biomat Sci-Polym E. 2011; 22:1509–1522.
59. Evenou F, Fujii T, Sakai Y. Spontaneous formation of stably-attached and 3D–organized hepatocyte aggregates on oxygen-permeable polydimethylsiloxane membranes having 3D microstructures. Biomedical Microdevices. 2010; 12:465–475. [PubMed: 20174871]
60. Martin I, Wendt D, Heberer M. The role of bioreactors in tissue engineering. Trends Biotechnol. 2004; 22:80–86. [PubMed: 14757042]
61. Wendt D, Riboldi SA, Cioffi M, Martin I. Bioreactors in tissue engineering: scientific challenges and clinical perspectives. Adv Biochem Eng/Biotechnol. 2009; 112:1–27.
62. Eniwumide JO, Lee DA, Bader DL. The development of a bioreactor to perfuse radially-confined hydrogel constructs: design and characterization of mass transport properties. Biorheology. 2009; 46:417–437. [PubMed: 19940357]
63. Hollingshead MG, Alley MC, Camalier RF, Abbott BJ, Mayo JG, Malspeis L, et al. In vivo cultivation of tumor cells in hollow fibers. Life Sci. 1995; 57:131–141. [PubMed: 7603295]
64. Casciari JJ, Hollingshead MG, Alley MC, Mayo JG, Malspeis L, Miyauchi S, et al. Growth and chemotherapeutic response of cells in a hollow-fiber in vitro solid tumor model. J Natl Cancer Inst. 1994; 86:1846–1852. [PubMed: 7990159]
65. Bettahalli NM, Vicente J, Moroni L, Higuera GA, van Blitterswijk CA, Wessling M, et al. Integration of hollow fiber membranes improves nutrient supply in three-dimensional tissue constructs. Acta Biomaterialia. 2011; 7:3312–3324. [PubMed: 21704736]
66. Gerlach JC, Lin YC, Brayfield CA, Minteer DM, Li H, Rubin JP, et al. Adipogenesis of human adipose-derived stem cells within three-dimensional hollow fiber-based bioreactors. Tissue Eng Part C Meth. 2012; 18:54–61.
67. Hay PD, Veitch AR, Smith MD, Cousins RB, Gaylor JD. Oxygen transfer in a diffusion-limited hollow fiber bioartificial liver. Artif Organs. 2000; 24:278–288. [PubMed: 10816201]
68. Shatford RA, Nyberg SL, Meier SJ, White JG, Payne WD, Hu WS, et al. Hepatocyte function in a hollow fiber bioreactor: a potential bioartificial liver. J Surgical Res. 1992; 53:549–557.

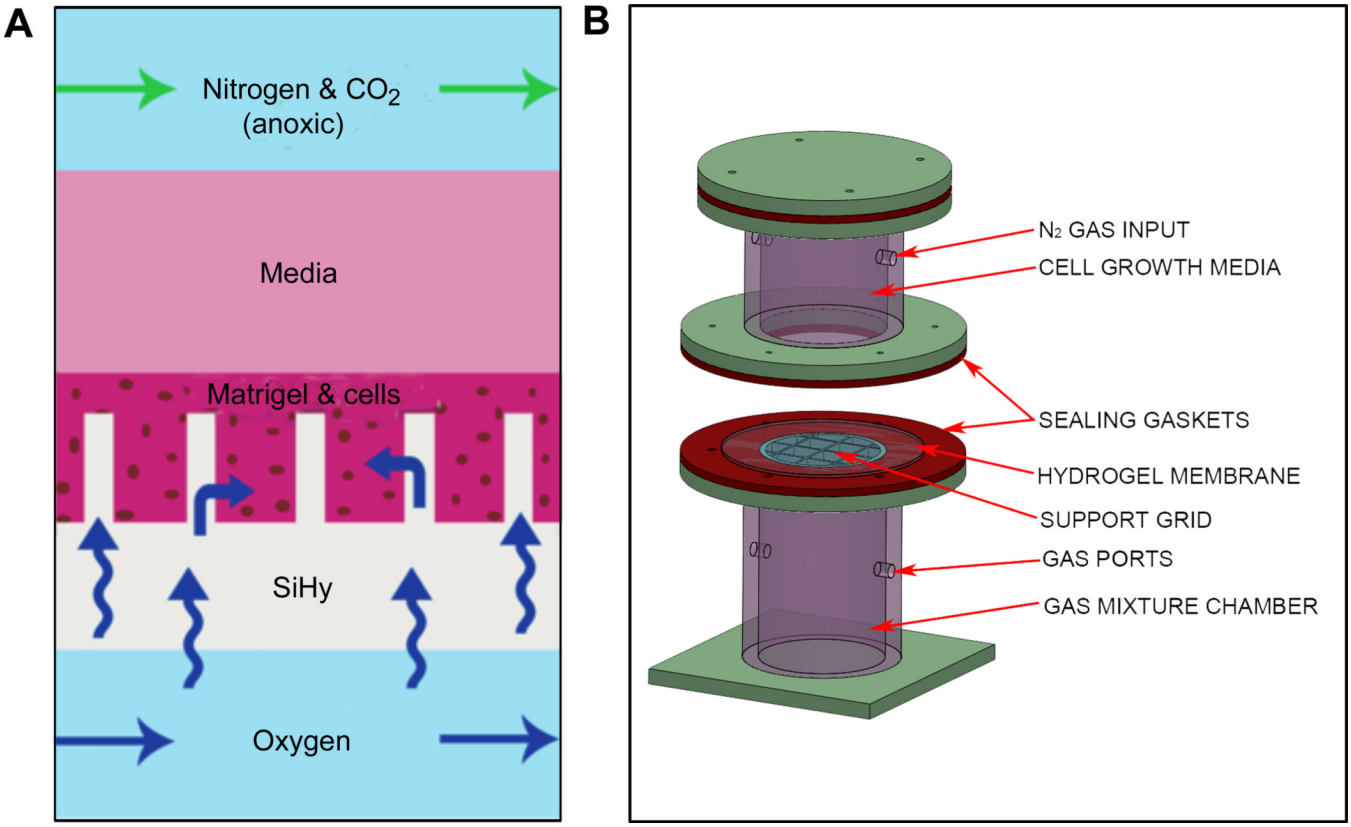

Fig. 1.

(A) Schematic showing the conceptual diffusion of O_2 through silicone hydrogel micropillars to oxygenate surrounding cells suspended in Matrigel basement membrane extract. (B) SolidWorks model of the constructed bioreactor system with mixed gas flowmeter input. The two flanged components sandwich the fabricated SiHy micropillar membrane, with cells and Matrigel loaded on top before adding media.

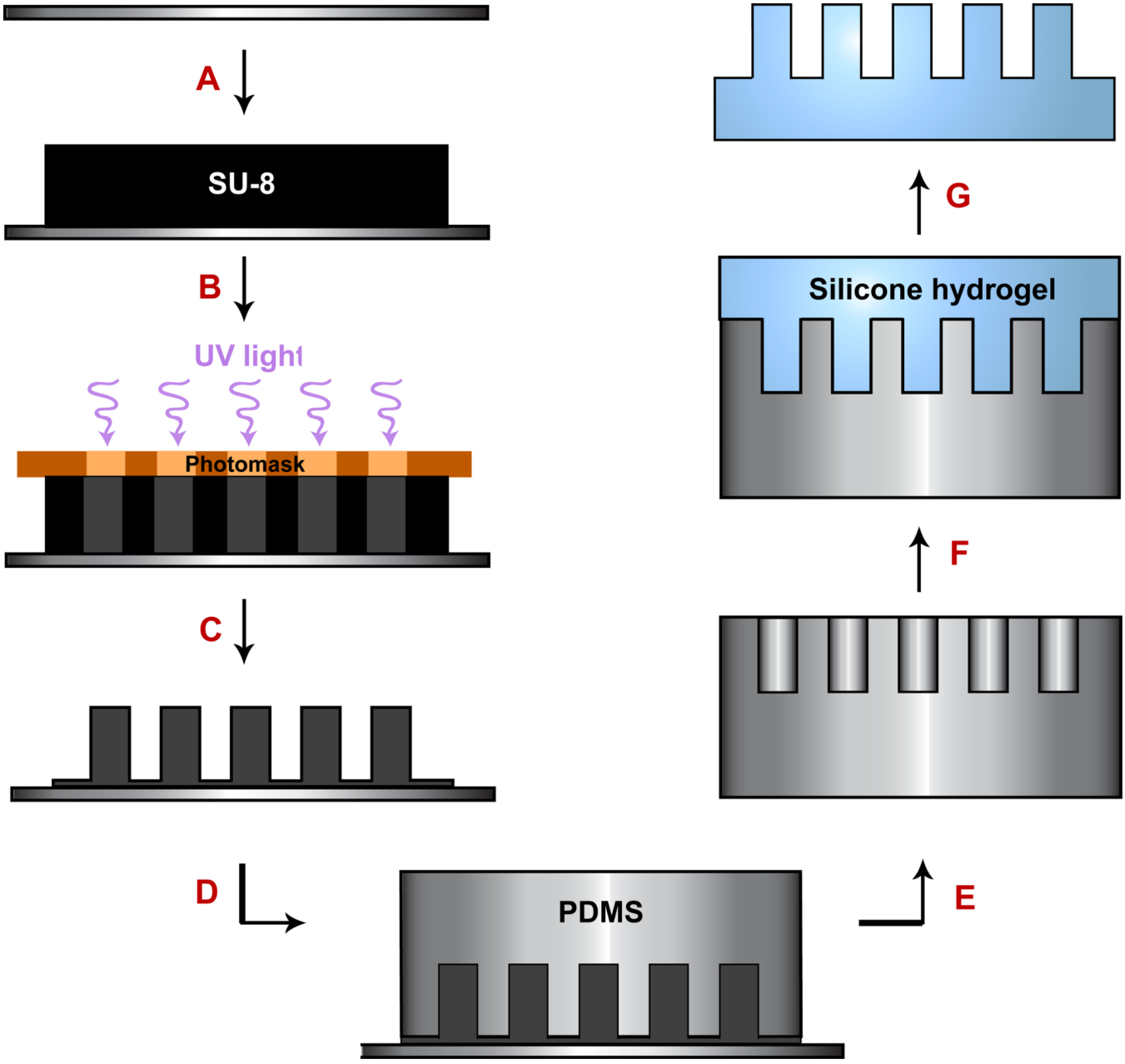

Fig. 2.

Process flow for silicone hydrogel fabrication. (A) A silicone wafer is baked at 200 °C (20 min) and pretreated with MCC Primer 80/20 to improve adhesion properties. Negative epoxy photoresist (SU-8 2150) is deposited onto the wafer by spinning. (B) A photomask is used to selectively expose areas of the SU-8 (creating the pillars) before a post exposure bake. (C) Unexposed SU-8 is removed during development, template is hard baked and silanized. (D) To create a negative mold, PDMS is cast on the SU-8 master. (E) Methanol is used to facilitate de-molding the PDMS mold. (F) A silicone hydrogel mixture is poured onto the negative PDMS mold and photopolymerized by exposure to high intensity UVC light (280 – 100 nm). (G) The completed silicone hydrogel membrane is de-molded and washed in acetone, followed by a gentle 24 h ethanol wash on an orbital shaker, then dried prior to incorporation into the bioreactor system.

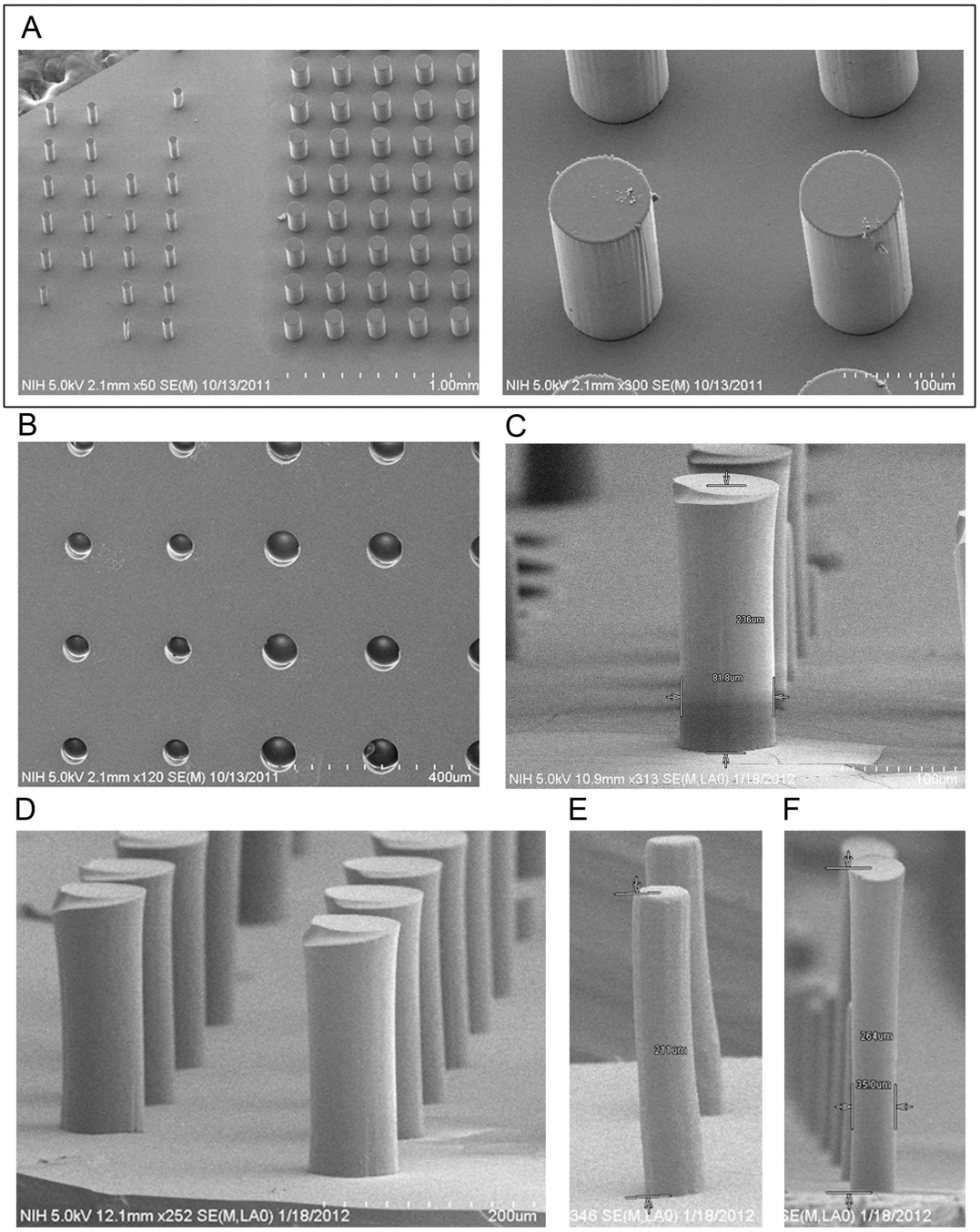

Fig. 3.

Scanning electron microscope (SEM) images of micropillars at different processing steps of silicone hydrogel fabrication outlined in Fig. 2. **(A)** SU-8 micropillar master mold. **(B)** Negative PDMS mold replicated from SU-8 master. **(C–F)** Silicone hydrogel micropillars cast from PDMS molds where **(E, F)** demonstrate the optimized micropillar dimensions that were achieved. Images are representative of usual results.

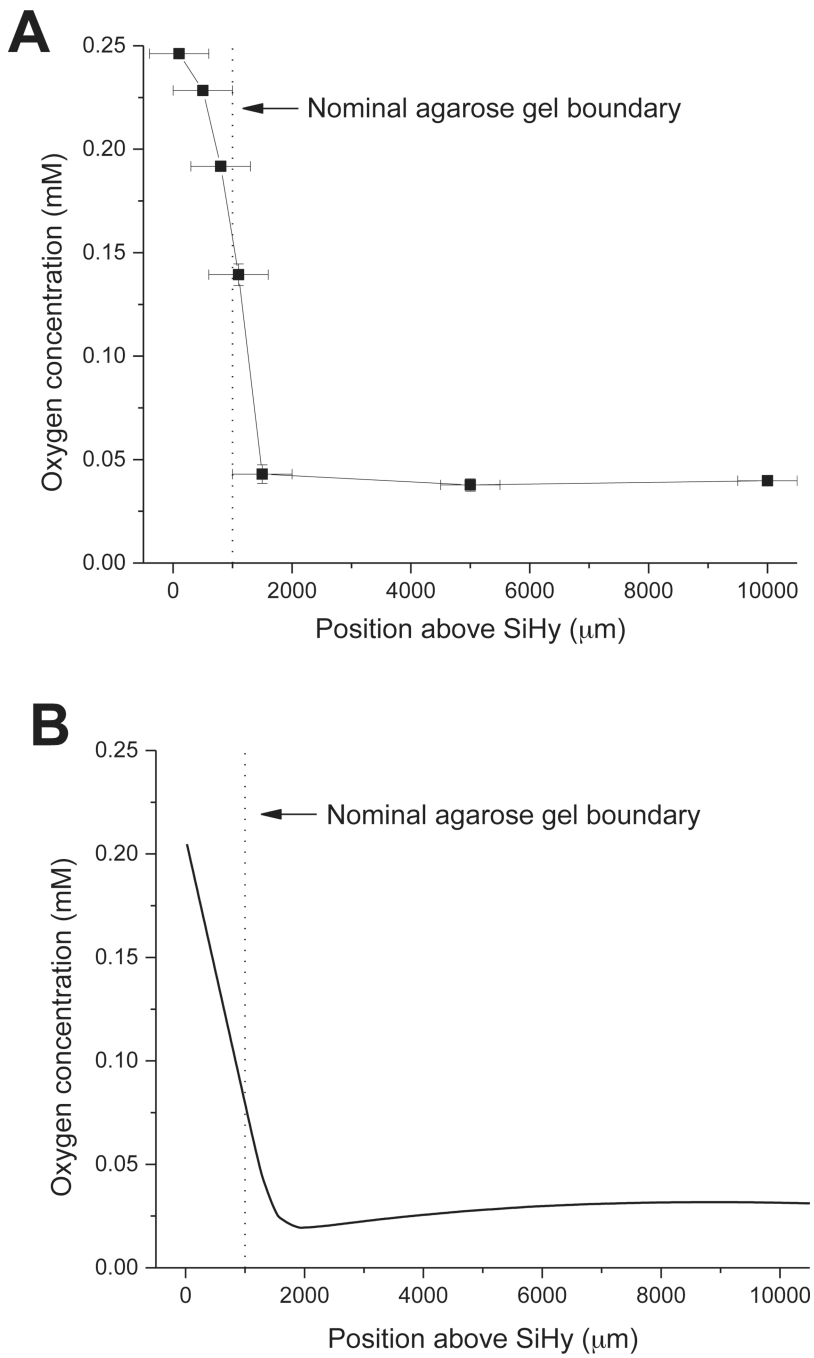

Fig. 4.

Measured **(A)** and calculated **(B)** equilibrium O_2 gradient in the bioreactor, using agar and water instead of Matrigel and culture media, as a function of distance away from a flat silicone hydrogel membrane. A) Experimental points are the values of oxygen concentration measured by a stationary sensor after equilibration (Fig S2), with horizontal error bars reflecting uncertainty due to sensor position and size, and vertical error bars reflecting long time-scale drift in measurement, likely mostly due to differences between liquid temperature and gas temperature. Other sources of error are not included. B) Average equilibrium oxygen gradient calculated for a 5 mm diameter cylindrical volume at the center the bioreactor, using a 2-D axisymmetric finite element model as described in text. Physical

constants are $D_{O2,SiHy} = 5\times10^{-9}$ m^2/s, $D_{O2,water} = 3\times10^{-9}$ m^2/s, SiHy/water partition coefficient = 8, O_2 mass transfer coefficient at the water/gas interface = 7×10^{-6} m/s. Nominal position of boundary between agar layer and water shown as a vertical dashed line in both graphs.

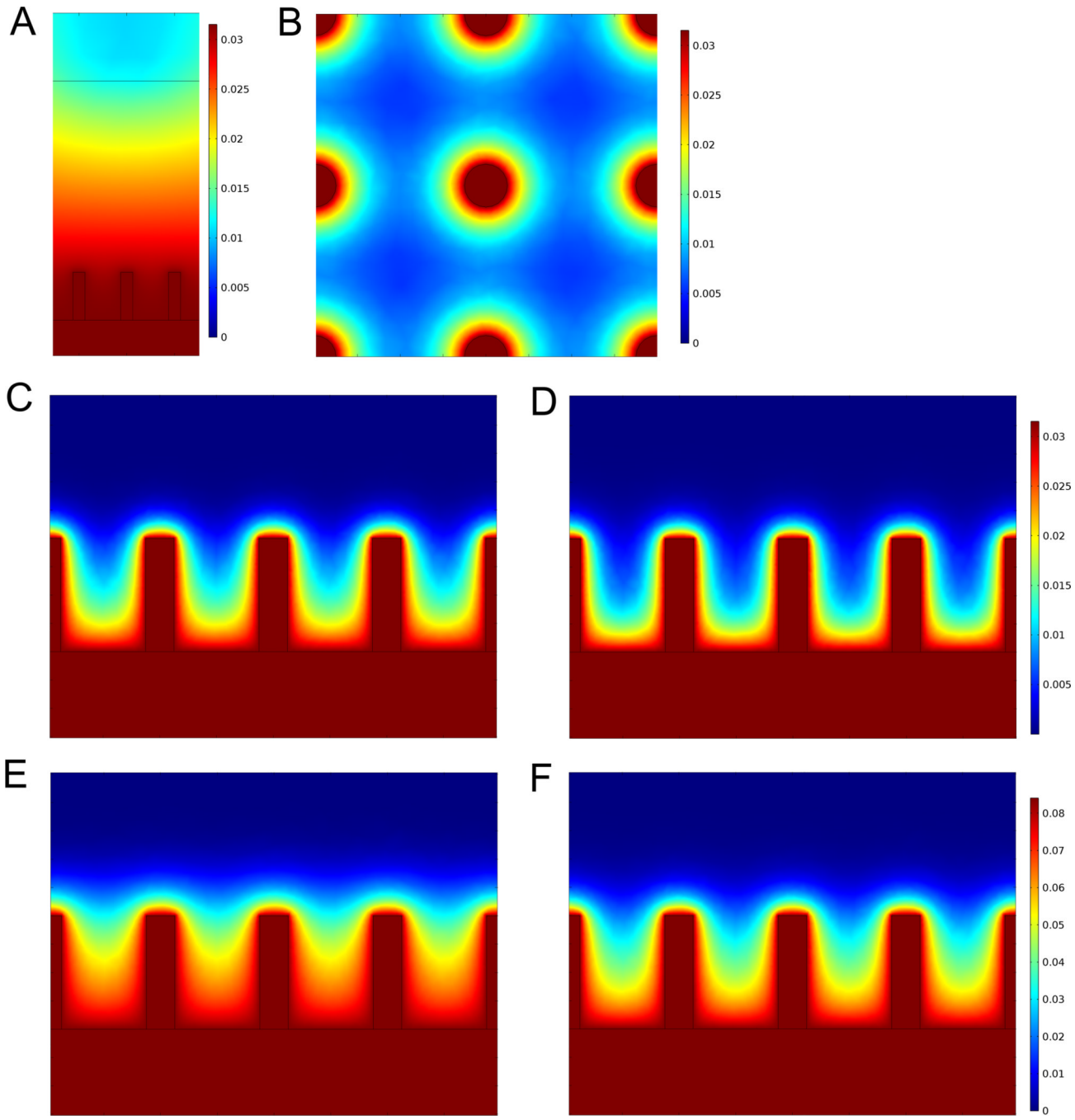

Fig. 5.

COMSOL Multiphysics simulation software was used for 3-D finite element modeling of steady state oxygen gradients around the micropillar array. Colorbar scales shown in mM concentration units. For a plane vertically transecting the pillars, steady-state O_2 concentration **(A)** without cellular consumption, and with cells filling the Matrigel volume for **(C,E)** low and **(D,F)** high rates of consumption (parameters given in text) for **(C,D)** 3% and **(E,F)** 8% O_2 source concentrations**(B)** O_2 concentration for a plane horizontally transecting the pillars 100 μm above the SiHy surface, for 3% O_2 source concentration and high cellular consumption.

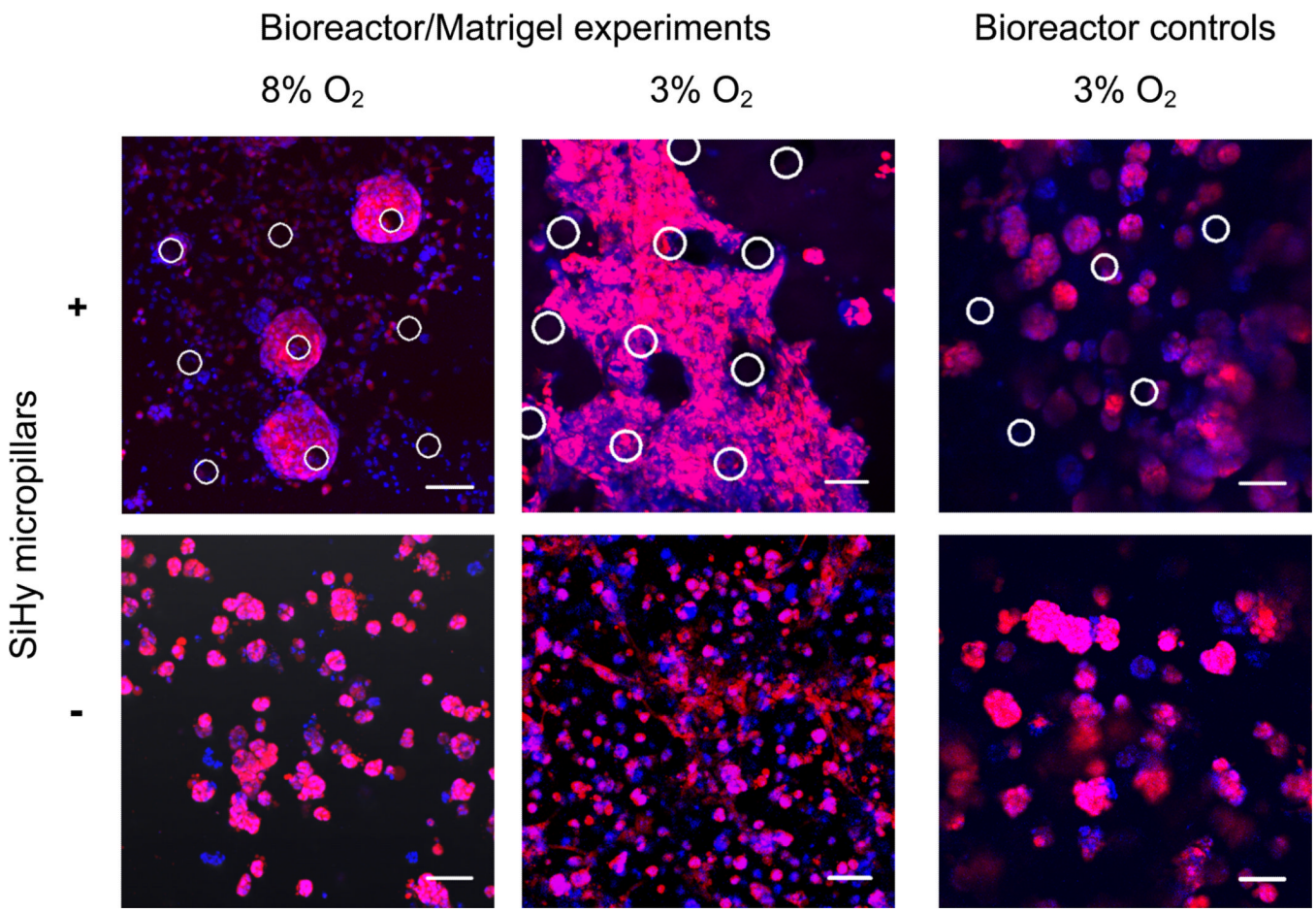

Fig. 6.

3-D cultures of OVCAR8-DsRed2 cells oxygenated via micropillars generate distinct culture geometries. The positions of the micropillars are shown as white circles. Images are maximum intensity projections of a range of z-values (200–250 μm z-stacks). Confocal images of 7 d bioreactor cultures in Matrigel with the upper bioreactor chamber maintained at 0% O_2 (95% N_2, 5% CO_2) and lower bioreactor chambers maintained at 3% (top center) and 8% O_2 (top left). Control culture geometries of cells grown in Matrigel for 7 days at 3% (bottom center) and 8% O_2 (bottom left) show smaller spheroidal morphologies. One type of bioreactor control experiment involved culturing cells in the bioreactor in the absence of an O_2 gradient (top right). Both chambers were kept at 3% O_2 for 7 d to serve as a bioreactor control. The second bioreactor control experiment involved an O_2 gradient, but used a flat SiHy membrane (bottom right). The top and bottom chambers were kept at 0% O_2 and 3% O_2, respectively. Scale bar, 100 μm.

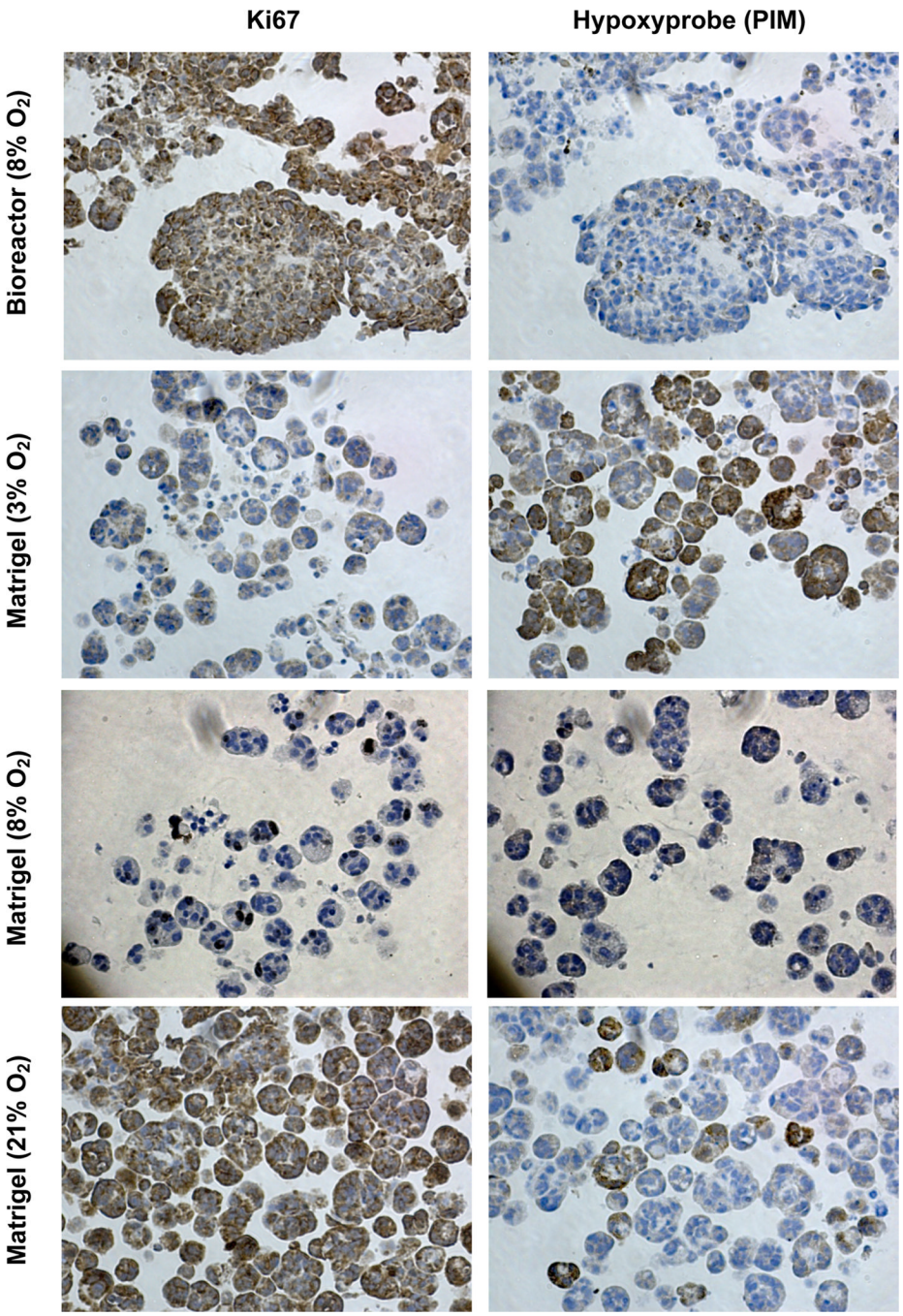

Fig. 7.

Tumor hypoxia and cell proliferation status in 3-D cell culture at different O_2 concentrations. OVCAR8-DsRed2 fluorescent cells were cultured for 7 days at 3, 8 and 21% O_2 in Matrigel and with 8% O_2 in the lower chamber of the bioreactor culture system. Cell proliferation and hypoxia staining were performed with Ki67 for detection of proliferating cells and pimonidazole hydrochloride (Hypoxyprobe) to detect hypoxia within cells, respectively. Increasing O_2 concentration showed a corresponding increase in Ki-67 staining and decrease in pimonidazole staining in 3-D Matrigel culture. The bioreactor culture demonstrates a difference in growth morphology compared to 3-D culture in Matrigel and

suggests that a lower O_2 tension is required to achieve hypoxic culture conditions more akin to *in vivo* conditions.

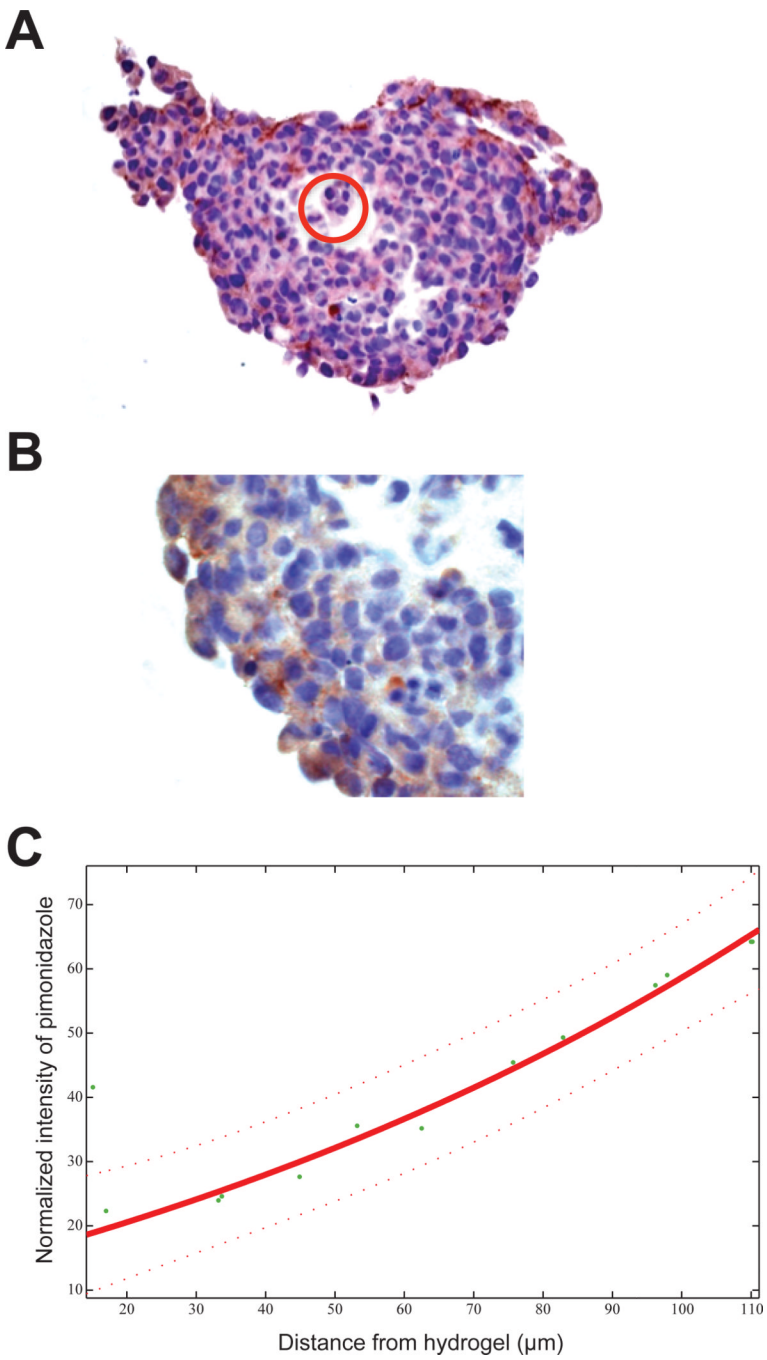

Fig. 8.

Inverse O_2 gradient exists within the tumor organoids cultured in the bioreactor system. **(A)** Pimonidazole staining of a tumor organoid (OVCAR8-dsRed2 cells) removed from a silicone hydrogel micropillar after a 7 d culture in the bioreactor system. The bottom chamber of the bioreactor was maintained at 3% O_2. The location of the micropillar passing through the organoid is circled. **(B)** Image highlighting the gradient in pimonidazole staining intensity used to generate the following **(C)** analysis of staining intensity (hypoxia) as a function of distance from the pillar (tumor organoid center).